

Spin-flip hot spots in ultrathin films of monovalent metals: Enhancement and anisotropy of the Elliott-Yafet parameter

Nguyen H. Long,* Phivos Mavropoulos,† Swantje Heers, Bernd Zimmermann, Yuriy Mokrousov, and Stefan Blügel
*Peter Grünberg Institut and Institute for Advanced Simulation,
 Forschungszentrum Jülich and JARA, D-52425 Jülich, Germany*

In contrast to the long-known fact that spin-flip hot spots, i.e., special \mathbf{k} -points on the Fermi surface showing a high spin-mixing parameter, do not occur in the bulk of monovalent (noble and alkali) metals, we found them on the surface Brillouin-zone boundary of ultrathin films of these metals. Density-functional calculations within the Korringa-Kohn-Rostoker Green function method for ultrathin (001) oriented Cu, Ag, and Au films of 10-layer thickness show that the region around the hot spots can have a substantial contribution, e.g. 52% in Au(001), to the integrated spin-mixing parameter, that could lead to a significant enhancement of the spin-relaxation rate or spin-Hall angle in thin films. Owing to the appearance of spin-flip hot-spots, a large anisotropy of the Elliott-Yafet parameter [50% for Au(001)] is also found in these systems. The findings are important for spintronics applications in which noble-metals are frequently used and in which the dimensionality of the sample is reduced.

PACS numbers: 72.25.Rb, 73.50.Bk, 72.25.Ba, 85.75.-d

I. INTRODUCTION

The term *spin-flip hot spots* was coined by Fabian and Das Sarma^{1,2} when, based on the Elliott-Yafet mechanism,^{3,4} they predicted a high spin-flip probability for electrons at certain special points on the Fermi surface of bulk Aluminium. The hot spots are formed by the spin-orbit interaction in the vicinity of band degeneracies or near-degeneracies, frequently occurring at the Brillouin-zone boundaries, high-symmetry lines or points of accidental degeneracy. On the other hand, hot spots should be absent in monovalent metals,^{1,2} because their Fermi surface is nearly spherical and in most cases does not cross the Brillouin-zone edge.

These conclusions were derived for the bulk.^{1,5,6} However, in the case of ultrathin films spin-flip hot spots may occur even in monovalent metals owing to the different shape of the surface Brillouin zone compared to the bulk. This is the main conclusion of the present paper, which we base on simple theoretical arguments and on a verification for (001) oriented ultrathin crystalline films of Cu, Ag, and Au as well as alkali metals. We adopt the structural model of free-standing films as generic for films that are deposited on, or sandwiched between, insulating materials, in particular concerning the electronic structure of the quantum-well states in the film. Our main focus is on the noble metals because of their frequent usage in spintronics applications as wires, contacts or probes. We investigate the contribution of the hot spots to the Elliott-Yafet parameter^{3,4} b^2 (defined below) as well as to its anisotropy. Our findings should be accounted for in spintronics applications where the hot spots play a role, such as for giant magnetoresistance, spin-Hall effect and spin dynamics.⁷⁻⁹

II. THEORY

We proceed with a short summary of the theoretical background.^{1,3,4} In non-magnetic systems with space-inversion symmetry and in the presence of the spin-orbit coupling the Bloch states at any \mathbf{k} -point are at least twofold degenerate and comprise a superposition of spin-up and spin-down states that is frequently called spin mixing:

$$\begin{aligned}\Psi_{\mathbf{k}}^+(\mathbf{r}) &= [a_{\mathbf{k}}(\mathbf{r})|\uparrow\rangle + b_{\mathbf{k}}(\mathbf{r})|\downarrow\rangle]e^{i\mathbf{k}\mathbf{r}} \\ \Psi_{\mathbf{k}}^-(\mathbf{r}) &= [a_{-\mathbf{k}}^*(\mathbf{r})|\downarrow\rangle - b_{-\mathbf{k}}^*(\mathbf{r})|\uparrow\rangle]e^{i\mathbf{k}\mathbf{r}}.\end{aligned}\quad (1)$$

Here, the spinors $|\uparrow\rangle$ and $|\downarrow\rangle$ are eigenvectors of the z -component Pauli matrix σ_z (given a chosen z -axis) and $a_{\mathbf{k}}(\mathbf{r})$ and $b_{\mathbf{k}}(\mathbf{r})$ are the lattice-periodic parts of the Bloch states and are denoted as the large and small spin-component, respectively, because they are chosen such that the norm of $a_{\mathbf{k}}$ is maximal and that of $b_{\mathbf{k}}$ is minimal (see below). The spin-expectation values of these partner states are $\mathbf{S}(\mathbf{k}) = \langle \Psi_{\mathbf{k}}^+ | \frac{\hbar}{2} \boldsymbol{\sigma} | \Psi_{\mathbf{k}}^+ \rangle = -\langle \Psi_{\mathbf{k}}^- | \frac{\hbar}{2} \boldsymbol{\sigma} | \Psi_{\mathbf{k}}^- \rangle$ with $\boldsymbol{\sigma}$ denoting the vector of Pauli matrices. The index “+” refers to the state with maximal z -component of the spin-expectation value $S_z(\mathbf{k}) = \hbar(\frac{1}{2} - b_{\mathbf{k}}^2)$, where $b_{\mathbf{k}}^2 := \int d^3r |b_{\mathbf{k}}(\mathbf{r})|^2 \in [0, \frac{1}{2}]$ defines the space-integrated spin-mixing parameter. Maximizing the value of $S_z(\mathbf{k})$ is done with respect to all possible linear combinations of the two degenerate states at \mathbf{k} , and it is obvious that one can choose a different pair of states in Eq. (1) by maximizing the projection of $\mathbf{S}(\mathbf{k})$ along any spin-quantization axis $\hat{\mathbf{s}}$ prescribed by the experimental conditions (e.g. by an external magnetic field or by the polarization direction of an injected spin current).^{10,11} The procedure for finding the wavefunctions that yield the maximal $\mathbf{S}(\mathbf{k})$ is given in the appendix. We will return to this freedom of choice of $\hat{\mathbf{s}}$ below when defining the anisotropy of the Elliott-Yafet parameter. The relation between the large

and small components of $\Psi_{\mathbf{k}}^-$ and $\Psi_{-\mathbf{k}}^+$ implied in Eq. (1), i.e. presence of the coefficients $a_{-\mathbf{k}}^*(\mathbf{r})$ and $-b_{-\mathbf{k}}^*(\mathbf{r})$ in the expression for $\Psi_{+\mathbf{k}}^-$, follows from time-reversal and space-inversion symmetry.^{3,4} It is also convenient to define the Elliott-Yafet parameter b^2 as the Fermi-surface average:

$$b^2 = \langle b_{\mathbf{k}}^2 \rangle_{\text{FS}} = \frac{1}{n(E_F)} \frac{1}{V_{\text{BZ}}} \int_{\text{FS}} \frac{d\Omega_{\mathbf{k}}}{\hbar v_{\mathbf{k}}} b_{\mathbf{k}}^2, \quad (2)$$

where $d\Omega_{\mathbf{k}}$ is the Fermi-surface element, $v_{\mathbf{k}}$ is the modulus of the Fermi velocity, $n(E_F)$ is the density of states at the Fermi level E_F , and V_{BZ} is the Brillouin-zone volume (or area in two dimensions).

The spin-mixing parameter $b_{\mathbf{k}}^2$ is the main quantity of interest in the analysis of many spin-flip related phenomena, as it reflects the deviation of a Bloch state from being a spin eigenstate. When $b_{\mathbf{k}}^2$ happens to be large (close to $\frac{1}{2}$), then the particular state has an almost completely mixed spin character.^{1,2,5} Concerning spin relaxation, an electron scattered into this state practically loses its spin character—for example, according to Elliott's approximation,³ the spin relaxation time T_1 is inversely proportional to the Elliott-Yafet parameter b^2 . Concerning the spin-Hall effect, such a state with large $b_{\mathbf{k}}^2$ is associated with a high value of the Berry curvature^{8,13} and exhibits thus a strong contribution to the conductivity tensor. The mixing $b_{\mathbf{k}}^2$ becomes large at, and close to, special points in the BZ, the spin-flip hot spots, that we are examining in the present work.

We should point out that the values of $b_{\mathbf{k}}^2$, as well as the integrated b^2 , depend on the direction of the spin-quantization axis $\hat{\mathbf{s}}$, because the matrix elements of the spin-flip part of the spin-orbit operator between Bloch states change with respect to the $\hat{\mathbf{s}}$ axis along which $\mathbf{S}(\mathbf{k})$ is maximized.^{10–12} Therefore we define the anisotropy of the Elliott-Yafet parameter as¹⁰

$$\mathcal{A}[b^2] = \frac{\max_{\hat{\mathbf{s}}} b^2(\hat{\mathbf{s}}) - \min_{\hat{\mathbf{s}}} b^2(\hat{\mathbf{s}})}{\min_{\hat{\mathbf{s}}} b^2(\hat{\mathbf{s}})} \quad (3)$$

by considering the maximum and minimum value with respect to all directions of $\hat{\mathbf{s}}$ in the unit sphere.

For bulk materials, this anisotropy effect, its microscopic origin and its relation to hot spots was analyzed in Refs. 10,11. It is obvious that the thin film geometry breaks the cubic symmetry and two surfaces, or generally, interfaces appear, and we expect that the value of b^2 will be different for spin-quantization axes $\hat{\mathbf{s}}$ chosen in the film plane ([100]-direction) or perpendicular to the plane [001]. This has been shown explicitly and attributed mainly to surface states for the transition-metal W(001) films in Ref. 12. Physical consequences of the anisotropy are, e.g., a variation of the spin-relaxation time or of the spin-Hall conductivity with respect to the direction of polarization of the spin current in the material, that corresponds to the polarization direction $\hat{\mathbf{s}}$ in the present theory.

The fact that spin-flip hot spots occur at points of degeneracy or near-degeneracy, in particular at the back-folded energy bands at the Brillouin-zone edge, follows

from a consideration of transitions from a band at energy $E_{\mathbf{k}}$ to a band at $E_{\mathbf{k}} + \Delta_{\mathbf{k}}$ of small inter-band separation $\Delta_{\mathbf{k}}$ under the action of the spin-orbit Hamiltonian.^{1,2,5} From these arguments it also follows that monovalent metals should not show spin-flip hot spots,^{1,2,5} since their almost spherical Fermi surface either does not cross the Brillouin-zone boundary (as for all alkali metals except Cs) or, if it crosses the boundary (as for the noble metals, forming a neck around the L -point), then it does so in a way that there occur no hot spots. The validity of the latter statement is shown and discussed in detail in Ref. 5.

However, the situation of monovalent metals changes when one considers ultrathin films. In this case the two-dimensional periodicity implies a surface Brillouin-zone, while the Fermi surface consists of rings occurring when the spherical Fermi surface of the bulk system is cut parallel to the surface plane at positions determined by the finite-size quantization of k_z due to films of finite thickness. This well-known effect is schematically demonstrated in Fig. 1a. Considering a (001) film, where the surface Brillouin-zone is a square, the larger of the Fermi rings exits the first Brillouin zone and a back-folding occurs (see the dashed lines and their back-folded counterparts in Fig. 1b). The back-folding, under action of the periodic potential, can form a weak degeneracy lifting at the Brillouin-zone edge, with the resulting states being energetically very close. But this is precisely the case when spin-flip hot spots occur under the action of the spin-orbit coupling between the near-degenerate states.

To what extent this actually happens in a realistic case depends on the exact shape of the Fermi surface, the number of film layers, the surface orientation, and of course the material. Here, we present *ab initio* results for Cu, Ag and Au (001) films of 10 layers thickness, where we find always an effect of considerable magnitude. This is in difference to alkali (001) thin films, where we find that the magnitude of the effect depends on the film thickness due to the weak spin-orbit coupling.

The electronic structure is calculated within the local density approximation to density-functional theory in the parametrization of Vosko *et al.*¹⁴ at experimental lattice parameters and ignoring surface relaxation. For our calculations we employ the full-potential Korringa-Kohn-Rostoker Green function method with an angular momentum cutoff of $l_{\text{max}} = 3$. The Fermi surfaces are interpolated from a mesh of 80×80 points in the surface Brillouin zone, resulting in approximately 9000 \mathbf{k} -points on the Fermi surface. Details on the formalism and implementation can be found in Refs. 15–17.

III. RESULTS AND DISCUSSION

Starting our analysis with the bulk properties, the spin-mixing parameter for bulk Cu and Au is well studied (for $\hat{\mathbf{s}} \parallel [001]$), e.g. in Ref. 15 and Ref. 18. It is long-known that the Fermi surfaces of the noble metals are

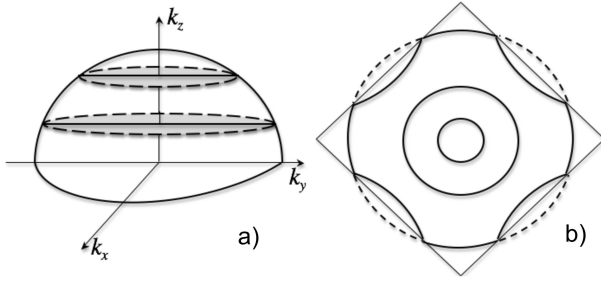


FIG. 1: Sketch of the ideal Fermi surface of a monovalent metal. (a) Spherical bulk Fermi surface; the circles shown at certain values of k_z correspond to the size-quantization of k_z in a film grown in the z -direction. (b) Fermi circles in a (001) film and the back-folding into the first surface Brillouin-zone, shown together with the crossed surface Brillouin-zone boundary. This schematic form of the Fermi surface is modified even in free-electron metals, especially if there is some d contribution at E_F , as we see in Fig. 2.

similar. The texture of $b_{\mathbf{k}}^2$ on the Fermi surfaces is also similar, but the magnitude is very different due to the much stronger spin-orbit coupling in Au. It is found that, for $\hat{s} \parallel [001]$, the value of $b_{\mathbf{k}}^2$ varies as a function of the position on the Fermi surface between 0.0005 and 0.002 in bulk Cu, between 0.0008 and 0.0025 in Ag, while in Au it clearly reaches much higher values varying between 0.01 and 0.045. It is also found that there are no hot spots on the noble-metal Fermi surfaces. The Fermi-surface average is calculated to be $b^2(\text{Cu}) = 0.0015$, $b^2(\text{Ag}) = 0.0017$, and $b^2(\text{Au}) = 0.03$. We also find that in the bulk of noble metals the cubic symmetry and the absence of hot spots makes the anisotropy of b^2 negligible (less than 0.1% comparing $\hat{s} \parallel [001]$, $[110]$ and $[111]$) but in the films it takes large values due to the hot spots, as we show below.

Now we examine the distribution of $b_{\mathbf{k}}^2$ on the Fermi surfaces of the ultrathin films. Fig. 2 (top and middle) illustrates the distribution of the spin-mixing parameter on the Fermi surface of a 10-layer Au(001) film for two spin-quantization axes, left panel along the $[001]$ direction and right one along the $[100]$ -direction. It is easily seen (see middle panel for finer detail) that spin hot-spots are found near the edge of the Brillouin zone. While for most \mathbf{k} -points inside the Brillouin zone the spin-mixing parameter has a value of less than 0.05, at the edge of the Brillouin zone it exhibits very high values reaching even the maximal value of fully spin-mixed states, $b_{\mathbf{k}}^2 = \frac{1}{2}$. The anisotropy of the spin-mixing parameter is already disclosed by the sheer observation of the difference between the color-coded textures of $b_{\mathbf{k}}^2$ in the left panel of Fig. 2 ($\hat{s} \parallel [001]$) and the right panel ($\hat{s} \parallel [100]$), especially if one focuses on the hot-spot. The symmetry of the distribution of $b_{\mathbf{k}}^2$ depends also on the choice of the spin-quantization axis. From Fig. 2 (top) it is obvious that the $[100]$ -direction lowers the symmetry with respect to the $[001]$ -direction leading to an asymmetric distribution of the values of $b_{\mathbf{k}}^2$.

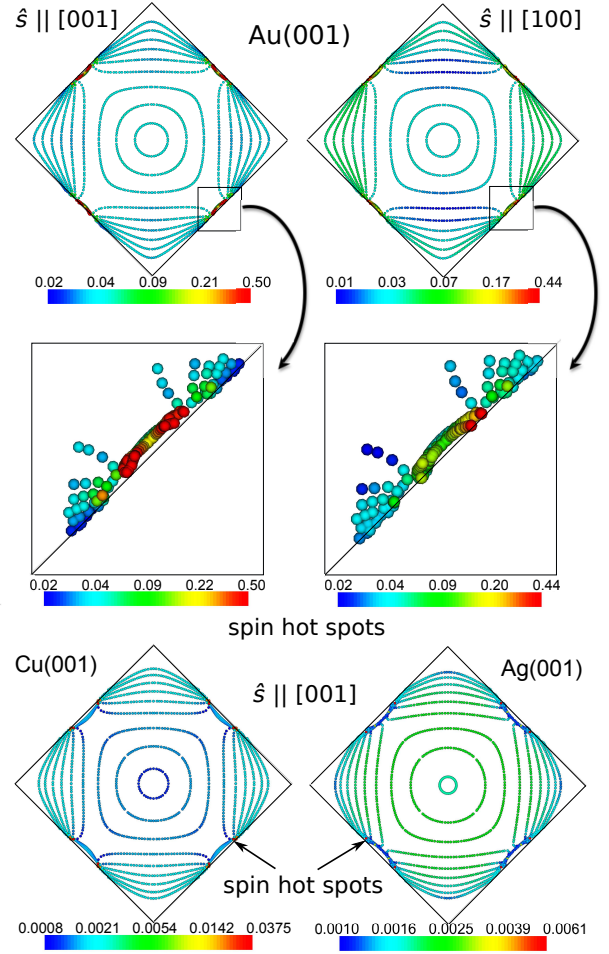


FIG. 2: (Color online) Top: Distribution of spin-mixing parameter on the Fermi surface of a 10 atomic layer thick Au(001) film with the spin-quantization axis along $[001]$, i.e. out of plane (left panel) and in-plane along the $[100]$ direction (right panel). The full surface Brillouin-zone is shown. Middle: Focus on the Brillouin-zone edge of Au(001) shown in the top panels in order to distinguish the extent of the hot spots. An asymmetry of distribution of $b_{\mathbf{k}}^2$ can be seen in the case of $\hat{s} \parallel [100]$ (right). Bottom: Distribution of spin-mixing parameter on the Fermi surface of a Cu(001) (left) and a Ag(001) (right) 10-layer film with the $\hat{s} \parallel [001]$ (out of plane).

Summing up over the Fermi surface, we obtain $b^2([001]) = 0.065$ for Au(001). This value is considerably higher than the value of 0.03 that we find for bulk Au or of 0.035 that we find for a 10-layer Au(111) film; (111) films show no hot-spots but have Rashba-type surface states^{19,20} causing an enhanced spin-mixing parameter.¹⁵ On the contrary, in the (001) thin films, there are no surface states at the Fermi level, yet the value of b^2 is higher. This demonstrates the importance of the spin-flip hot-spots in this case. To estimate the contribution of hot-spots to the total spin-mixing parameter, we perform the integration in Eq. (2) only for the \mathbf{k} -points belonging to a small area around the hot-spots and quantify the area by its contribution to the density of states at E_F . We find

that an area contributing to 4% of $n(E_F)$ contributes by 41% to the b^2 for Cu; an area contributing to 9% of the DOS contributes to 14% of the b^2 for Ag; and an area contributing to 10% of $n(E_F)$ contributes by 52% to the b^2 for Au.

In the case that \hat{s} is along the [100] direction (Fig. 2, right-side top and middle panels) the values of $b_{\mathbf{k}}^2$ change; the maximum value is then 0.44 and the integrated one is $b^2([100]) = 0.042$ for Au. Among all directions of \hat{s} in the unit sphere we find that b^2 is maximal for $\hat{s} \parallel [001]$ and minimal for $\hat{s} \parallel [100]$ and thus we obtain for the anisotropy $\mathcal{A} = [b^2([001]) - b^2([100])] / b^2([100])$ a value of 50% for Au. This value is gigantic compared to the negligible anisotropy in the bulk of noble metals, and it is comparable in magnitude to the anisotropy in e.g. W(001) films,¹² where it arises from surface states, or to the anisotropy in bulk hcp Os (59%)¹⁰ where it arises from larger spin-flip hot areas. However, the present value is still an order of magnitude lower than the one of bulk hcp Hf (830%) where it arises from hot loops at the edge of the hcp Brillouin zone, which occur when the Fermi surface crosses the hexagonal Brillouin zone edge in hcp metals.¹⁰

The Fermi surfaces of the 10-layer Cu(001) and Ag(001) films are shown in the bottom panel of Fig. 2 together with $b_{\mathbf{k}}^2([001])$ in a color code. Just as in Au, also here the spin-flip hot-spots are present at the surface Brillouin-zone edge. The hot spots are, however, less intense due to the weaker spin-orbit coupling of Cu and Ag. The anisotropy \mathcal{A} is found to be 30% and 8% for 10-layer Cu(001) and Ag(001) films, respectively. The Fermi surface integrated $b^2([001])$ in Cu(001) is 0.002, which exceeds the value of 0.0016 that we find for the 10-layer (111) film in spite of the Rashba surface states of the latter, i.e., we see the same qualitative behavior that we observed when comparing Au(001) with Au(111); the same holds for Ag. Our results are summarized in Table I.

We also examine shortly the question of stability of the hot spots and of the anisotropy with respect to temperature. We gain a qualitative picture by calculating b^2 and \mathcal{A} at energies slightly different than E_F , in particular $E_F \pm 13.6$ meV (13.6 meV correspond to a temperature of 157 Kelvin). Our results are summarized in Table II and show that there is a quantitative change of the values in this energy window, but from an order-of-magnitude point of view the results are stable. The changes arise because the position and intensity of the hot spots varies as the constant-energy surfaces change with energy.

From the results of Tables I and II it seems that Ag has an unexpectedly low value of b^2 and of \mathcal{A} , comparable to Cu or even smaller, despite the stronger spin-orbit coupling of Ag compared to Cu. We were able to trace this back to the well-known low position of the d -bands of Ag with respect to E_F , compared to Cu or Au, by conducting a numerical experiment. Acting with a repulsive projection potential, we shifted the Ag d -bands higher in energy by 1.2 eV, positioning d band edge at 1.5 eV

Metal	$b^2 \times 10^2$				\mathcal{A}
	bulk	film $\hat{s} \parallel [001]$	film $\hat{s} \parallel [100]$	film $\hat{s} \parallel [110]$	
Cu	0.15	0.241	0.186	0.186	30%
Ag	0.17	0.193	0.179	0.179	8%
Au	3.0	6.53	4.34	4.50	49%

TABLE I: Values of the Elliott-Yafet parameter ($\times 10^2$) in bulk and in 10-layer Cu, Ag and Au (001)-films. In the case of the films, the values are given for three directions of \hat{s} with respect to the crystallographic axes ([001] corresponds to the direction of \hat{s} normal to the film surface). The anisotropy values \mathcal{A} correspond to the films. The anisotropy in bulk is less than 0.1%.

Metal	Energy	$b^2 \times 10^2$		\mathcal{A}
		$\hat{s} \parallel [001]$	$\hat{s} \parallel [100]$	
Cu	$E_F - 13.6$ meV	0.275	0.200	37%
	E_F	0.241	0.186	29%
	$E_F + 13.6$ meV	0.447	0.259	72%
Ag	$E_F - 13.6$ meV	0.249	0.200	24%
	E_F	0.193	0.179	8%
	$E_F + 13.6$ meV	0.246	0.200	23%
Au	$E_F - 13.6$ meV	7.36	4.56	61%
	E_F	6.53	4.34	50%
	$E_F + 13.6$ meV	6.01	4.12	46%

TABLE II: Variance of the Elliott-Yafet parameter and its anisotropy with respect to the energy around E_F for Cu, Ag, and Au 10-layer (001) films. Shown are the values of $10^2 \times b^2$ for $\hat{s} \parallel [001]$ and $[100]$ and the anisotropy at E_F and $E_F \pm 13.6$ meV. Note that 13.6 meV corresponds to a temperature of 157 K.

under E_F , as is approximately the calculated value for Cu and Au. The value of b^2 increased then by an order of magnitude and the anisotropy increased to 140%. We conclude that the d admixture of the Fermi surface contributes to the value of b^2 significantly.

Concluding the discussion on the noble-metal films, we comment on the absence of hot spots in (111) oriented thin films. Part of the reason is that the (111) oriented atomic planes of fcc crystals are more close-packed than the (001) oriented atomic planes, resulting in a larger surface Brillouin-zone area by a factor $2/\sqrt{3}$. The fact that the (111) surface Brillouin-zone is hexagonal, and in this sense closer in shape to the maximal circle forming the equator of the bulk Fermi surface, is another aspect. As a result of both, the projection of the bulk Fermi surface almost fits into the surface Brillouin-zone, leaving only little room for crossing the zone boundary. Whether such crossings appear and lead to hot spots has to be tested for each material and thickness separately, but as we find, it is not the case for the ultrathin (111) oriented noble metal films.

Finally, for completeness, we briefly discuss the spin-mixing enhancement in alkali-metal thin films, even though they are typically not used in spintronics devices. Although the electronic structure of alkali metals con-

sists basically of s -electrons, even for the alkali metals the Fermi surface has a non-vanishing p and d character that is responsible for spin-orbit coupling with strength $\xi_\ell = \langle \ell | \frac{\hbar}{2m^2 c^2 r} \frac{dV}{dr} | \ell \rangle$, with the angular momentum state $|\ell\rangle$ being $\ell = 1$ or $\ell = 2$ for p or d wavefunctions, respectively. The Coulomb potential of the nucleus that causes most of the spin-orbit coupling is well screened by the filled shells of the core electrons, contrary to the noble metals, where a larger part of the screening is done by the valence electrons and by the not-fully-localized d band. Additionally, the d character of the alkali-metal Fermi surfaces is less pronounced in comparison to noble metals (with the exception of Ag) and the spin-orbit coupling of the d states at E_F in the noble metals is strong because of the high localization of the d bands. As a consequence, the spin-orbit strength in alkali metals is expected to be lower than in the noble metals. Still, we found that at some film thicknesses, e.g. 10 layers of Na(001), K(001), and Rb(001), the Fermi surface without spin-orbit coupling is degenerate at the Brillouin-zone edge meaning that the first Fourier component of the periodic potential vanishes (at least to numerical accuracy, which we have cross-checked using the full-potential linearized augmented plane wave method²¹). In this case spin-orbit coupling causes a splitting with full spin mixing when \hat{s} is perpendicular to the film, i.e. hot spots with $b_{\mathbf{k}}^2 = \frac{1}{2}$ emerge at the Brillouin-zone edge. Yet the magnitude of $b_{\mathbf{k}}^2$ drops very quickly as the bands separate with increasing distance from the edge, e.g. in Rb(001) we find that $b_{\mathbf{k}}^2 = 0.02$ already at a distance of $0.0005 \times \frac{2\pi}{a_{\text{lat}}}$ (where a_{lat} is the lattice constant). Thus in the alkali metal films almost the entire magnitude value of b^2 comes from a very small region around the hot spots (similarly to the case of bulk Al¹) and the anisotropy, that is generally more pronounced at and around the hot spots, is significant. In 10-layer films, where hot spots are present, we find the following maximal and minimal values: $b^2([001]) = 0.086 \times 10^{-2}$, $b^2([110]) = 0.025 \times 10^{-2}$ and $\mathcal{A} = 244\%$ for Na(001); $b^2([001]) = 0.11 \times 10^{-2}$, $b^2([110]) = 0.039 \times 10^{-2}$ and $\mathcal{A} = 182\%$ for K(001); and $b^2([001]) = 0.45 \times 10^{-2}$, $b^2([110]) = 0.16 \times 10^{-2}$ and $\mathcal{A} = 181\%$ for Rb(001).

IV. SUMMARY

In summary, we have shown that the Fermi surface of monovalent metals in an ultrathin film geometry can show spin-flip hot spots as the Fermi rings cross the surface Brillouin-zone boundary. This is in contrast to the bulk of such metals, where it is known^{1,2,5} that hot spots do not occur, as the Fermi surface is included within the Brillouin zone. We have furthermore shown that the hot spots contribute to large anisotropy values of the spin-mixing parameter with respect to the relative orientation between the spin-quantization axis and the crystallographic directions. Since the presence of hot spots

strongly influences the spin-relaxation time or the spin-Hall conductivity, our findings can have consequences in spintronics applications, in particular since ultrathin noble-metal films are used to transmit or probe spin currents. The calculated anisotropy can very likely lead to a variation of the spin-relaxation time with respect to the spin-polarization direction of the spin current in experiments and it is important to average this quantity for the estimation of those transport properties in polycrystalline samples.

Acknowledgments

We acknowledge funding from the project MO 1731/3-1, the programme SPP 1538 SpinCaT of the Deutsche Forschungsgemeinschaft and from the HGF-YIG VH-NG-513 project of the Helmholtz Gemeinschaft. We acknowledge the Jülich Supercomputing Centre for providing us with computational time.

Appendix

Here we present the algorithm for choosing the linear combination of degenerate states that maximizes the value of $S_z(\mathbf{k})$ [see the discussion after Eq. (1)]. Given two orthogonal solutions at \mathbf{k} , say $\Psi_{\mathbf{k}}^{(1)}$ and $\Psi_{\mathbf{k}}^{(2)}$ (that are found in the process of solving the eigenvalue problem), any linear combination $\Psi_{\mathbf{k}} = c_{\mathbf{k}}^{(1)} \Psi_{\mathbf{k}}^{(1)} + c_{\mathbf{k}}^{(2)} \Psi_{\mathbf{k}}^{(2)}$ is still a Bloch eigenfunction of the Hamiltonian, as long as $c_{\mathbf{k}}^{(1,2)}$ are complex numbers independent of \mathbf{r} . Since by normalization $|c_{\mathbf{k}}^{(1)}|^2 + |c_{\mathbf{k}}^{(2)}|^2 = 1$, and since a global phase factor is irrelevant, we can replace the two complex numbers by two real parameters $\alpha_{\mathbf{k}}$ and $\beta_{\mathbf{k}}$ such that $\Psi_{\mathbf{k}} = \cos \frac{\alpha_{\mathbf{k}}}{2} \Psi_{\mathbf{k}}^{(1)} + e^{i\beta_{\mathbf{k}}} \sin \frac{\alpha_{\mathbf{k}}}{2} \Psi_{\mathbf{k}}^{(2)}$. Using a shorthand notation we define the spin expectation value along z for this linear combination as $S = \langle \Psi_{\mathbf{k}} | \frac{\hbar}{2} \sigma_z | \Psi_{\mathbf{k}} \rangle$ and analogously $S_1 = \langle \Psi_{\mathbf{k}}^{(1)} | \frac{\hbar}{2} \sigma_z | \Psi_{\mathbf{k}}^{(1)} \rangle$, $S_2 = \langle \Psi_{\mathbf{k}}^{(2)} | \frac{\hbar}{2} \sigma_z | \Psi_{\mathbf{k}}^{(2)} \rangle$ as well as the cross-term $S_{12} = \langle \Psi_{\mathbf{k}}^{(1)} | \frac{\hbar}{2} \sigma_z | \Psi_{\mathbf{k}}^{(2)} \rangle$. Then we have $S = S_1 \cos^2 \frac{\alpha_{\mathbf{k}}}{2} + S_2 \sin^2 \frac{\alpha_{\mathbf{k}}}{2} + (e^{i\beta_{\mathbf{k}}} S_{12} + e^{-i\beta_{\mathbf{k}}} S_{12}^*) \cos \frac{\alpha_{\mathbf{k}}}{2} \sin \frac{\alpha_{\mathbf{k}}}{2}$. Maximizing or minimizing this expression with respect to $\alpha_{\mathbf{k}}$ and $\beta_{\mathbf{k}}$ gives by definition $\Psi_{\mathbf{k}} = \Psi_{\mathbf{k}}^+$ or $\Psi_{\mathbf{k}} = \Psi_{\mathbf{k}}^-$, i.e., the sought-after states. Demanding that the derivatives with respect to $\alpha_{\mathbf{k}}$ and $\beta_{\mathbf{k}}$ vanish, we arrive at the result $\beta_{\mathbf{k}} = -S_{12}/|S_{12}| + n\pi \equiv -\arg(S_{12}) + n\pi$ (n integer), $\alpha_{\mathbf{k}} = \pm \arctan[2|S_{12}|/(S_1 - S_2)]$ (or $\alpha_{\mathbf{k}} = \pm\pi$, if $S_1 = S_2$), which maximizes or minimizes the $S_z(\mathbf{k})$ and which we use for the $\Psi_{\mathbf{k}}^\pm$. Obviously this has to be repeated for every \mathbf{k} on the Fermi surface. The same procedure can be followed for maximizing the spin along any SQA \hat{s} by replacing σ_z by $\boldsymbol{\sigma} \cdot \hat{s}$.

-
- * Electronic address: H.Nguyen@fz-juelich.de
† Electronic address: Ph.Mavropoulos@fz-juelich.de
- ¹ J. Fabian and S. Das Sarma, Phys. Rev. Lett. **81**, 5624 (1998).
 - ² J. Fabian and S. Das Sarma, Phys. Rev. Lett. **83**, 1211 (1999).
 - ³ R. J. Elliott, Phys. Rev. **96**, 266 (1954).
 - ⁴ Y. Yafet, in *Solid State Physics*, edited by F. Seitz and D. Turnbull, Academic, New York, vol. **14**, 2 (1963).
 - ⁵ J. Fabian and S. Das Sarma, J. Appl. Phys. **85**, 5075 (1999).
 - ⁶ J. Fabian and S. Das Sarma, J. Vac. Sci. Techn. B **4**, 1708 (1999).
 - ⁷ I. Žutić, J. Fabian, D. Sarma, Rev. Mod. Phys. **76**, 323 (2004).
 - ⁸ Y.K. Kato, R.C. Myers, A.C. Gossard, and D.D. Awschalom, Science **306**, 1910 (2004); J. Sinova, D. Culcer, Q. Niu, N.A. Sinitsyn, T. Jungwirth, and A.H. MacDonald, Phys. Rev. Lett. **92**, 126603 (2004).
 - ⁹ D. Steiauf and M. Fähnle, Phys. Rev. B **79**, 140401 (2009).
 - ¹⁰ B. Zimmermann, P. Mavropoulos, S. Heers, N. H. Long, S. Blügel and Y. Mokrousov, Phys. Rev. Lett. **109**, 236603 (2012).
 - ¹¹ Y. Mokrousov, H. Zhang, F. Freimuth, B. Zimmermann, N. H. Long, J. Weischenberg, I. Souza, P. Mavropoulos and S. Blügel, J. Phys.: Condens. Matter **25**, 163201 (2013).
 - ¹² N. H. Long, P. Mavropoulos, B. Zimmermann, S. Heers, D.S.G. Bauer, S. Blügel, and Y. Mokrousov, Phys. Rev. B **87**, 224420 (2013).
 - ¹³ M. Gradhand, D. V. Fedorov, F. Pientka, P. Zahn, I. Mertig and B. L. Györfy, Phys. Rev. B **84**, 075113 (2011).
 - ¹⁴ S. H. Vosko, L. Wilk, and M. Nusair, Can. J. Phys. **58**, 1200 (1980).
 - ¹⁵ S. Heers, PhD Thesis, RWTH Aachen University (2011); <http://darwin.bth.rwth-aachen.de/opus3/volltexte/2011/3827/>
 - ¹⁶ N. Papanikolaou, R. Zeller, and P. H. Dederichs, J. Phys.: Condens. Matter **14**, 2799 (2002); see also <http://www.kkr-gf.org>.
 - ¹⁷ N. Stefanou and R. Zeller, J. Phys.: Condens. Matter **3**, 7599 (1991); N. Stefanou, H. Akai, and R. Zeller, Comput. Phys. Commun. **60**, 231 (1990).
 - ¹⁸ M. Gradhand, M. Czerner, D. V. Fedorov, P. Zahn, B. Y. Yavorsky, L. Szunyogh and I. Mertig, Phys. Rev. B **80**, 224413 (2009).
 - ¹⁹ S. LaShell, B. A. McDougall and E. Jensen, Phys. Rev. Lett. **77**, 3419 (1996).
 - ²⁰ J. Henk, A. Ernst and P. Bruno, Phys. Rev. B **68**, 165416 (2003).
 - ²¹ We used the FLEUR code, <http://www.flapw.de>.